Fluid Dynamics Simulation and Temperature Gradient Validation along a Greenhouse Temperature Gradient

Sung Kyeom Kim
Kyungpook National University
Hee Ju Lee
National Institute of Horticultural and Herbals Science
Seung Hwan Wi
National Institute of Horticultural and Herbal Science
Seong-Won Lee
Jeonbuk National University
ILHWAN Seo (ihseo@jbnu.ac.kr)
Jeonbuk National University https://orcid.org/0000-0003-1062-3132

Research article

Keywords: Climate change, Computational fluid dynamics, Temperature gradient greenhouse, Physiological disturbances

Posted Date: September 17th, 2020

DOI: https://doi.org/10.21203/rs.3.rs-55291/v1

Abstract

Background: Climate change is increasing the vulnerability of horticultural crop cultivation and production. It is urgent to study such extreme weather phenomena (heatwave, drought, etc.), and in particular, to evaluate crop productivity according to temperature change. For this purpose, the crop physiological response to temperature change in simulated weather conditions was studied. However, there is a limitation in artificial light wavelength, which requires experiments to be carried out in protected facilities or open fields. In this study, we simulated temperature differences with computational fluid dynamics (CFD) in tunnel-type greenhouses. They can create temperature gradients and improve the accuracy of CFD with vertically and horizontally measured temperature profiles. The growth and physiological response of Kimchi cabbage were examined and validated using a temperature gradient within a semi-closed plastic tunnel.

Results: Correlation coefficients of measured heights were: 1.120, 0.597, and 0.459. Root mean square error was below 0.1025, which means the CFD simulation values were highly accurate. The error analysis showed that it was possible to accurately predict temperature gradients change within a semi-closed tunnel-type greenhouse using CFD techniques. CFD results showed an average error of 0.597°C compared to field monitoring results. The maximum temperature difference of GTG was 5.7°C, suggesting a well-controlled set point (6°C difference between outside conditions and inside conditions of GTG). In a cloudy day, the gradient temperature of GTG was well maintained by the set differential temperature (dT), which suggests that the set dT was not precisely and accurately performed in GTG of a sunny day. There was a significant difference in the growth, net photosynthetic rate, transpiration rate, and Ci concentration along with temperature differences in GTG.

Conclusions: CFD can simulate temperature gradient distribution in a tunnel-type greenhouse and predict the temperature difference for equipment with different specifications. These facilities can be used in climate change-related studies, such as assessment of crop production area optimization, crop physiological response to temperature, vulnerability assessment of crop production under increasing temperatures, or extreme weather.

Background

Earth's temperature increased by an average of 0.7 °C during the past century. Since 1980, the temperature increase rate is rising twice as rapidly in Korea. Air temperature is predicted to increase with approximately 6.0 °C by 2100. According to the representative concentration pathway (RCP) 8.5 climate change (CC) scenario from Korea Meteorological Administration, CO_2 concentration is expected to increase to 940 μmol/mol, and the precipitation to increase by 20.4% compared to current levels. It is forecasted that CC and the resulting extreme weather in the tropical climate zone will harm horticultural crop production in the future. Increased CO_2 concentration is expected to enhance the photosynthesis efficiency of C3 plants and lead to higher productivity. Higher temperatures may also enhance crop growth, mainly through extending the growing season. In the present climate, this applies especially for the spring when light intensity is high but temperatures are too low for crop growth [1]. Most greenhouse studies have been able to demonstrate the optimum temperature for plant growth and temperatures at which high- and low-temperature injury occur. For example, tomato plants grow well at mean daily temperature of 15 °C to 25 °C but are damaged under suboptimal temperature conditions. This differs according to the cultivar used and other environmental conditions such as solar radiation [2]. Various studies investigated the impact of climate changes on crop productivity. They simulated the impact of climate change (elevated CO_2, temperature, and water deficit) on red and white grapevine growth in three consecutive growing seasons. This included the effect of elevated CO_2 concentration, temperature, and water deficit on growth, water status, and yield quality of grapevine cultivars [3, 4]. A large number of studies have investigated the response of various crop systems to both high CO_2 and temperature [5]. Carbon balance, partitioning dry matters, and photosynthetic acclimation in fruit-bearing grapevine, grown under simulated CC scenarios in GTG, were also studied [6]. Studies of vegetable crops found that growth, photosynthesis, and chlorophyll fluorescence of Kimchi cabbage responds to high temperature [7, 8]. Also, temperature gradient research reported that tomato crop growth and development responds to a vertical temperature gradient in a semi-closed greenhouse [9].

Experimental studies using GCG and GTG, some aiming to study photosynthetic acclimation, a phenomenon that leads to decreased photosynthetic capacity under long-term exposures to elevated CO_2, have been conducted [10]. However, there is a lack of information on the specification and performance of facilities and devices for temperature gradient implication in an open field or protected tunnels. Scientists and engineers in agricultural, biological, and ecological sciences have developed a variety of controlled environmental systems for experimental research of plant responses to their environmental conditions [11]. A greenhouse is designed to create a microclimate that allows adequate crop growth and to isolate it from adverse external conditions. To develop a climate control scheme for a greenhouse, it is necessary to obtain a mathematical model, which describes accurately the dynamic behavior of climate variables [12]. The appropriate distribution of climatic parameters, such as temperature, humidity, and CO_2 concentration in greenhouses are the major factors that influence crop growth uniformity. Thus, investigating the internal climatic pattern is of great importance for improving the design of greenhouse ventilation and cooling, or heating systems. Climatic gradients at plant level within the greenhouse are the main concern of growers. The prediction of such gradients was found to be difficult because the complex nature of such gradients.

CFD (Computational Fluid Dynamics) is based on aerodynamic approaches in terms of heat, gas, dust concentrations, and flow patterns. It can accurately analyze and gather both quantitative and qualitative data inside and outside the agricultural facility. Although the field experiments in greenhouse conditions are highly important to understand the actual pattern, the specific environmental factors are limited when the sensing equipment has been installed with a limited number of points. The installed equipment can only measure within a limited area and the monitoring data can be distorted compared to the actual situation. The internal aerodynamic problems cannot be solved only by field experiments. This is due to the invisible airflow that should be properly interpreted to understand the change of internal environmental factors. Therefore, it is possible to identify environmental problems, obtain improvement measures, and suggest structural enhancement plans through a process that analyzes the internal flow and thermal environment distribution inside the experimental greenhouse. This could be done using a verified CFD simulation model and field monitoring.

CFD has been actively used to solve internal environmental problems of agricultural facilities such as greenhouses and livestock houses. CFD model can be applied in various approaches in the agricultural sector [13]. It analyzes the internal greenhouse environmental factors according to the characteristics of the different entrances [14]. CFD can evaluate greenhouse wind pressure, too [15]. Internal environmental conditions in three different types of naturally ventilated greenhouses were analyzed using a two-dimensional transient CFD simulation [16].

There is a lack of information on GTG of CFD case study and validation of growth and physiological crop response to the temperature gradient. Thus, the crop physiological response to temperature change using artificial weather was studied. However, there is a limitation of GTG artificial light wavelength, which requires experiments to be carried out in protected facilities or open fields. The objective of this research is to interpret the internal thermal pattern of the greenhouse temperature gradient and to establish its usability in greenhouse conditions. An indoor temperature and humidity monitoring were performed for three different levels of the greenhouse temperature gradient. A three-dimensional CFD model with the same structural configuration was designed for precise analysis of ventilation, heating, external environments, and internal structure. The CFD model was validated by comparing it with field-monitored temperature distributions. It was used to analyze the internal environmental conditions of the greenhouse temperature gradient.

Methods

Specification of the greenhouse temperature gradient (GTG)

There are three GTGs in the National Horticultural and Herbal Science Institute located in Wanju (35°16'N, 127°02'E, 32 m a. s. l.). The experiments were carried out in one of the GTGs (Fig. 1-a and c). GTG's specifications and characters are shown in Table 1. The GTG is a semi-open tunnel type with a plastic cover material (Ethylene Tetra Fluoro Ethylene (ETFE), 0.1 mm

thin) that has light transiency greater than 89%. The tunnel is a galvanized round iron pipe designed in a Korean standard operation procedure, which means that the shade inside the GTG is below 10%. The GTG's temperature gradient was designed using the environmental control system equipped with a data logger (CR1000x, Campbell Sci. Co., USA), programable relays (SDM-CD16, Campbell Sci. Co., USA), six ventilation fans, and a heater (Fig. 1-b). The controlling algorithm is shown in Fig. 2. It was used with the six ventilation fans (EK-4070, Hanil Co., Korea) and the hot-blast-heating style heater (Sunart-6000, NS Tech. Co., Korea). The programmable relays were controlled by a mechanical language (supplementary data: Table 1). The ventilation fan control pattern was divided into photo and dark periods with a radiation intensity of 250 w/m^2 (correctable). The ventilation fans were programmed as follows: 2 (one fan open), 5 (two fans open), 1 and 3 (four fans open), 4 and 6 (six fans open). When the radiation intensity was 250 w/m^2 or greater, all six ventilation fans were open and controlled in the above sequence according to the temperature difference change (dT). When the radiation intensity was 250 w/m^2 or less, the ventilation fans were controlled according to the change in dT. During the night, ventilation fans 4 and 6 were not used due to the rapid temperature decrease when the ventilation fans were open. Thus, to avoid rapid temperature decrease, ventilation fans 4 and 6 were not used during the dark-period. The activity of hot air heater was also divided into photo and dark periods based on the radiation intensity of 250 w/m^2. This was done to control its activity in the same way as the ventilation fans. When the solar radiation was 250 w/m^2 or greater, the hot air heater was not operational regardless of dT. When the solar radiation was 250 w/m^2 or less, the hot air heater was working according to the change in dT.

Table 1
Specification of the temperature gradient

Classification	Specification	Remarks
Type	Semi-closed plastic tunnel	0.1 mm thin ETFE cover materials
Size	With × length × height: 3.0 × 25 × 2.5 m	Cultivation area: 75 m^2
Ventilation part	Six ventilation fans and one micro fan South bound: open (no cover materials)	Fan size and power: Φ450mm, 140W 72 m^3/min, 1400 rpm
Control panel	Data logger (CR-1000×, Campbell Co., USA) Control relay (SDM-16 Campbell Co., USA)	Control program developed CR basic (Supplementary data)
Sensors	Outside: temperature, radiation, wind speed Inside: 6 temperature and humidity sensors (HMP50, Visala Co. Ltd., Finland)	Temperature sensor using the control set point (dT)
Heater	Air heating generator type: 6.4 kW, 504 kcal/hr	-
Duct	Aluminum cylinder type, 1 m interval each Φ20 mm hole	Supply of warm airflow into the tunnel

Table 2
Data of the 90 temperature sensors, t-types thermocouple type, along the temperature gradient

Id	Horizontal position	Vertical position	Calibration (mult/offset)
1	0.75/0.0 m from west/south bounds	40 mm above ground	1.0357/−1.2438
2	0.75/0.0 m from west/south bounds	80 mm above ground	1.0013/−0.3994
3	0.75/0.0 m from west /south bounds	120 mm above ground	0.9883/−0.0389
4	1.50/0.0 m from west/south bounds	40 mm above ground	1.0067/−0.5921
5	1.50/0.0 m from west/south bounds	80 mm above ground	0.9805/−0.0460
6	1.50/0.0 m from west/south bounds	120 mm above ground	1.0049/−0.4966
7	2.25/0.0 m from west/south bounds	40 mm above ground	0.9941/−0.2751
8	2.25/0.0 m from west/south bounds	80 mm above ground	0.9692/+0.3615
9	2.25/0.0 m from west/south bounds	120 mm above ground	0.9971/−0.2857
10	0.75/2.6 m from west/south bounds	40 mm above ground	0.9925/−0.3045
11	0.75/2.6 m from west/south bounds	80 mm above ground	1.0319/−1.0142
12	0.75/2.6 m from west/south bounds	120 mm above ground	1.0047/−0.3836
13	1.50/2.6 m from west/south bounds	40 mm above ground	0.9944/−0.2243
14	1.50/2.6 m from west/south bounds	80 mm above ground	1.0126/−0.6051
15	1.50/2.6 m from west/south bounds	120 mm above ground	1.0218/−1.0136
16	2.25/2.6 m from west/south bounds	40 mm above ground	1.0170/−0.6732
17	2.25/2.6 m from west/south bounds	80 mm above ground	0.9948/−0.2323
18	2.25/2.6 m from west/south bounds	120 mm above ground	0.9878/+0.0034
19	0.75/5.2 m from west/south bounds	40 mm above ground	0.9948/−0.1523
20	0.75/5.2 m from west/south bounds	80 mm above ground	1.0283/−0.9789
21	0.75/5.2 m from west/south bounds	120 mm above ground	1.0177/−0.6842
22	1.50/5.2 m from west/south bounds	40 mm above ground	0.9823/+0.1985
23	1.50/5.2 m from west/south bounds	80 mm above ground	1.0096/−0.6164
24	1.50/5.2 m from west/south bounds	120 mm above ground	0.9722/+0.2447
25	2.25/5.2 m from west/south bounds	40 mm above ground	1.0114/−0.5938
26	2.25/5.2 m from west/south bounds	80 mm above ground	0.9996/−0.3683
27	2.25/5.2 m from west/south bounds	120 mm above ground	0.9625/+0.5936
28	0.75/7.8 m from west/south bounds	40 mm above ground	1.0188/−0.6930
29	0.75/7.8 m from west/south bounds	80 mm above ground	0.9899/−0.1394
30	0.75/7.8 m from west/south bounds	120 mm above ground	1.0458/−1.2025
31	1.50/7.8 m from west/south bounds	40 mm above ground	0.9833/−0.0298
32	1.50/7.8 m from west/south bounds	80 mm above ground	1.0159/−0.5487

Id	Horizontal position	Vertical position	Calibration (mult/offset)
33	1.50/7.8 m from west/south bounds	120 mm above ground	0.9798/+0.253
34	2.25/7.8 m from west/south bounds	40 mm above ground	0.9821/+0.0391
35	2.25/7.8 m from west/south bounds	80 mm above ground	1.0103/−0.6011
36	2.25/7.8 m from west/south bounds	120 mm above ground	0.9895/−0.0077
37	0.75/10.4 m from west/south bounds	40 mm above ground	1.0367/−1.0002
38	0.75/10.4 m from west/south bounds	80 mm above ground	1.0183/−0.5289
39	0.75/10.4 m from west/south bounds	120 mm above ground	0.9591/+0.4496
40	1.50/10.4 m from west/south bounds	40 mm above ground	1.0242/−0.8694
41	1.50/10.4 m from west/south bounds	80 mm above ground	1.0111/−0.5008
42	1.50/10.4 m from west/south bounds	120 mm above ground	1.0095/−0.3858
43	2.25/10.4 m from west/south bounds	40 mm above ground	1.0247/−0.8098
44	2.25/10.4 m from west/south bounds	80 mm above ground	0.9717/+0.2589
45	2.25/10.4 m from west/south bounds	120 mm above ground	1.0158/−0.8162
46	0.75/13.0 m from west/south bounds	40 mm above ground	1.0488/−1.1811
47	0.75/13.0 m from west/south bounds	80 mm above ground	0.9987/−0.1443
48	0.75/13.0 m from west/south bounds	120 mm above ground	1.0146/−0.5592
49	1.50/13.0 m from west/south bounds	40 mm above ground	0.9885/−0.0738
50	1.50/13.0 m from west/south bounds	80 mm above ground	0.9935/−0.2285
51	1.50/13.0 m from west/south bounds	120 mm above ground	1.0461/−1.1217
52	2.25/13.0 m from west/south bounds	40 mm above ground	1.0006/−0.1847
53	2.25/13.0 m from west/south bounds	80 mm above ground	1.0202/−0.7249
54	2.25/13.0 m from west/south bounds	120 mm above ground	0.9905/−0.2023
55	0.75/15.6 m from west/south bounds	40 mm above ground	0.9987/−0.2943
56	0.75/15.6 m from west/south bounds	80 mm above ground	1.0483/−1.2470
57	0.75/15.6 m from west/south bounds	120 mm above ground	1.0022/−0.1591
58	1.50/15.6 m from west/south bounds	40 mm above ground	0.9934/−0.3223
59	1.50/15.6 m from west/south bounds	80 mm above ground	1.0144/−0.6743
60	1.50/15.6 m from west/south bounds	120 mm above ground	0.9996/−0.2445
61	2.25/15.6 m from west/south bounds	40 mm above ground	1.0314/−0.4951
62	2.25/15.6 m from west/south bounds	80 mm above ground	1.0740/−1.4455
63	2.25/15.6 m from west/south bounds	120 mm above ground	1.0485/−1.1447
64	0.75/18.2 m from west/south bounds	40 mm above ground	1.0366/−0.9855
65	0.75/18.2 m from west/south bounds	80 mm above ground	1.0633/−1.2981

Id	Horizontal position	Vertical position	Calibration (mult/offset)
66	0.75/18.2 m from west/south bounds	120 mm above ground	1.0294/−0.4598
67	1.50/18.2 m from west/south bounds	40 mm above ground	1.0728/−1.4485
68	1.50/18.2 m from west/south bounds	80 mm above ground	1.0782/−1.7169
69	1.50/18.2 m from west/south bounds	120 mm above ground	1.0544/−1.2247
70	2.25/18.2 m from west/south bounds	40 mm above ground	1.0311/−0.4657
71	2.25/18.2 m from west/south bounds	80 mm above ground	1.0890/−1.6974
72	2.25/18.2 m from west/south bounds	120 mm above ground	1.0066/−0.0738
73	0.75/20.8 m from west/south bounds	40 mm above ground	1.0818/−1.9707
74	0.75/20.8 m from west/south bounds	80 mm above ground	1.0352/−0.8282
75	0.75/20.8 m from west/south bounds	120 mm above ground	1.0214/−0.4066
76	1.50/20.8 m from west/south bounds	40 mm above ground	1.0740/−1.3739
77	1.50/20.8 m from west/south bounds	80 mm above ground	1.0291/−0.4022
78	1.50/20.8 m from west/south bounds	120 mm above ground	1.0600 /−1.2875
79	2.25/20.8 m from west/south bounds	40 mm above ground	1.0815/−1.7041
80	2.25/20.8 m from west/south bounds	80 mm above ground	1.0204/−0.1374
81	2.25/20.8 m from west/south bounds	120 mm above ground	1.0761/−1.4562
82	0.75/23.4 m from west/south bounds	40 mm above ground	1.0777/−1.7012
83	0.75/23.4 m from west/south bounds	80 mm above ground	1.0366/−0.8495
84	0.75/23.4 m from west/south bounds	120 mm above ground	1.0729/−1.5541
85	1.50/23.4 m from west/south bounds	40 mm above ground	1.0507/−0.9506
86	1.50/23.4 m from west/south bounds	80 mm above ground	1.0560/−1.1320
87	1.50/23.4 m from west/south bounds	120 mm above ground	1.0836/−1.8775
88	2.25/23.4 m from west/south bounds	40 mm above ground	1.0436/−1.0155
89	2.25/23.4 m from west/south bounds	80 mm above ground	1.0120/−0.0735
90	2.25/23.4 m from west/south bounds	120 mm above ground	1.0732/−1.3549

Measurement of outside environmental factors and temperature profiles in the GTG

To measure the actual GTG temperature and profile it vertically and horizontally, 90 thermocouple temperature sensors were installed inside it (Table 3, supplementary data: Fig. 1). A total of 27 (sensor ID 1–27) temperature sensors were installed outside GTG at 5.2 m distance and the area was designated as A zone. Another 27 temperature sensors (sensor ID 28–54) were installed at 5.2 to 13.0 m distance outside GTG and that area was designated as B zone. Finally, a total of 27 temperature sensors (sensor ID 55–90) were installed at a distance of 13.0 to 25.0 m outside GTG, and the area was designated as C zone. The vertical and horizontal GTG temperatures were automatically measured from a data logger (CR-1000x, Campbell. Co. Ltd., USA) for one-hour intervals from February 2 to February 28, 2019. The 90 self-made t-type thermocouple temperature sensors used a standard thermometer as reference (No. 1, SATO. Co. Ltd., Japan). This was done to improve the sensor's accuracy and precision through temperature calibration in a constant temperature water tank. The

multi-value and offset values of the calibration formula are presented in Table 3. The temperature sensors from the outside area were grouped by their temperature difference or the temperature gradient. The daily change of vertical and horizontal temperature distributions was analyzed for two days (one cloudy and one sunny day). An agricultural weather station facility (CR1000x, Campbell Sci. Co., USA) was installed in GTG external environment to measure the solar radiation (CMP3, Kipp & Zonnen B. V., Co. Ltd., The Netherlands), outside temperature and relative humidity (HMP155A, Vaisala Co. Ltd., Finland), and wind speed and direction (M05103, R.M. Company., USA).

Table 3
Profiles of measured air temperatures during the cloudy and sunny days along the temperature gradient

Sensor ID grouping		Daily mean temp. (°C)		Photoperiod temp. (°C)		Dark period temp. (°C)	
		Cloudy	Sunny	Cloudy	Sunny	Cloudy	Sunny
A	1–9	7.5 ± 0.3g[z]	6.3 ± 0.4 g	8.5 ± 0.3f	11.0 ± 0.3d	6.8 ± 0.3 g	2.9 ± 0.4f
	10–18	8.2 ± 0.2gf	7.3 ± 0.4f	9.3 ± 0.2e	12.4 ± 0.7c	7.4 ± 0.2 fg	3.6 ± 0.3f
	19–27	8.8 ± 0.5 g	8.0 ± 0.7e	9.8 ± 0.4e	13.1 ± 0.9bc	8.1 ± 0.5f	4.4 ± 0.6e
B	28–36	9.6 ± 0.5d	8.3 ± 0.6e	10.6 ± 0.d	12.3 ± 1.6c	8.9 ± 0.6e	5.4 ± 0.8d
	37–45	10.7 ± 1.0d	9.0 ± 1.0d	11.6 ± 0.9c	12.4 ± 1.0c	10.1 ± 1.0d	6.6 ± 1.1c
	46–54	10.7 ± 0.6d	9.2 ± 0.7 cd	11.7 ± 0.6c	13.2 ± 0.9bc	10.0 ± 0.7d	6.4 ± 0.6c
C	55–63	11.2 ± 0.5 cd	9.8 ± 0.6bc	12.2 ± 0.5bc	13.7 ± 0.7ab	10.5 ± 0.5 cd	6.9 ± 0.5bc
	64–72	11.8 ± 0.6bc	10.0 ± 0.6b	12.7 ± 0.5b	13.7 ± 0.9ab	11.1 ± 0.6bc	7.5 ± 0.6b
	73–81	13.1 ± 1.4a	10.9 ± 1.2a	14.0 ± 1.4a	13.7 ± 1.0ab	12.4 ± 1.5a	8.9 ± 1.6a
	82–90	12.4 ± 0.8b	10.9 ± 0.6a	13.5 ± 0.7a	14.5 ± 0.9a	11.5 ± 0.8b	8.4 ± 1.0a
Significance[y]		***	***	***	***	***	***

[z]The letters represent the significance of Duncan's multiple range test at p = 0.05. Mean ± standard deviation.

[y]***P ≤ 0.001.

Table 4
Boundary conditions used for the validation of CFD model

Contents	Values
Number of meshes	About 2.3 million (Tetrahedron)
Boundary conditions	Velocity inlet 1.4 m/s in one small fan and 4 m/s in one large fan Pressure inlet
Turbulence model	Standard k-ε model
Outside temperature	281.96 °K
Initial temperature	284.46 °K
Heating pipe	1.8 m/s at the end of the two pipes with 353.16 °K

Table 5
Validation of CFD simulation data and measured air temperature along the temperature gradient

Conditions		Slope	R^2	Estimated rising temperature for 25 m	Average error	Standard deviation
0.4 m	Field	0.213	0.996	5.33	1.120	0.640
	CFD	0.289	0.990	7.23		
0.8 m	Field	0.280	0.881	7.00	0.597	0.472
	CFD	0.299	0.979	7.48		
1.2 m	Field	0.266	0.947	6.65	0.459	0.526
	CFD	0.296	0.984	7.40		

Cfd Case Study And Specification Of Gtg

The CFD model is a tool for numerical analysis of non-linear partial differential equations for fluid flow phenomena with Navier-Stokes equations. It has been used to analyze heat transfer, multiphase flow analysis, and chemical reactions along with the fluid flow. The greenhouse temperature gradient was designed for analysis of indoor environments using space-claim (ver. 19.2., ANSYS Inc., USA). Figure 3 and Fig. 4 show the structural configuration of the CFD model. It has seven exhausting fans creating negative pressure ventilation (including one constantly operational fan and six temporally operational fans) and an open wall on the opposite side. To enhance the accuracy of the internal airflow analysis, cabbage was used as porous media with the same interval in the greenhouse as in the CFD model. Considering the economic efficiency of mesh design, aerodynamically important parts were designed with a dense mesh for a sophisticated airflow analysis. The total number of meshes is about 230 million. The simulation of the designed CFD model was carried out using ANSYS Fluent (ver. 19.2, ANSYS Inc., USA). Table 1 shows the boundary conditions used for CFD model validation based on the field monitoring results. Based on the negative pressure ventilation system, outside cold air was entering through the open-end wall, while the two-pipe heating system was operational at each side wall, exhausting heated to 80 °C air through the hole-type inlets.

Field monitoring data was used for validation of the CFD simulation model. The field experiments have been conducted from February 2nd to February 28th, 2019. The measurements were done at one-hour intervals using 90 temperature sensors. The obtained total 45,180 measurements were analyzed to extract appropriate data for CFD validation. CFD simulation can be validated only in a steady-state condition. However, field monitored environmental data had continuously changing temperature, wind direction, wind speed, etc. Therefore, field data with a relatively small temporal variation of air temperature was utilized. For the CFD validation, the mean absolute error (MAE) and the root mean square error (RMSE) were calculated. They were compared with the field monitored data and CFD-computed data.

$$\mathrm{MAE} = \frac{1}{n}\Sigma_{i=1}^{n}\left|T_{field} - T_{CFD}\right|$$

$$\mathrm{RMSE} = \sqrt{\frac{\Sigma_{i=1}^{n}\left(T_{field} - T_{CFD}\right)^2}{n}}$$

Using the validated CFD model, the internal airflow, temperature distribution, and ventilation efficiency were evaluated at heights of 0.4 m, 0.8 m, and 1.2 m from the floor bottom. TGD (Tracer Gas Decay) method was used to evaluate regional ventilation efficiency. The method tracks gas concentration reduction after opening the ventilation system. Thus, the

regional ventilation efficiency of CFD was calculated using TGD to reduce CO_2 concentration at the initial condition to 2,000 ppm.

Validation of Kimchi cabbage physiological responses and growth in GTG

At 28 days after sowing, the cv. Bulam No. 3 (Farm Hannong Co, Korea) Kimchi cabbage (*Brassica rapa* L. ssp. *Pekinensis*) transplants were planted in a completely randomized block design. It combined three replications with a planting density of 3–4 plant/m^2 in zones A, B, and C. At 58 days after transplanting (DAT), Kimchi cabbage were randomly sampled (n = 3) in each temperature zone to evaluate its growth. The measured variables were: maximum leaf width and length, number of leaves, leaf area, fresh weight, SPAD value, stomatal conductivity, and leaf temperature. Leaf area was measured using a leaf area meter (LI-3100C, LI-COR, Inc., USA). SPAD was measured at a random point on the outer green area of Kimchi cabbage leaves using an optical instrument (SPAD-502, Konica Minolta, Tokyo, Japan). The stomatal conductivity and leaf temperature were measured with a leaf porometer (SC-1-80, Decagon Devices, Inc., USA) after randomly selecting three Kimchi cabbage plants from each temperature zone. At the 38 DAT, the photosynthesis of three Kimchi cabbage leaves chosen randomly was measured along the temperature gradient (A, B, and C zone) using a portable photosynthesis system. The portable Li-COR gas exchange system (LI-6400XT, LI-COR, Inc., USA) maintained the flow rate and photosynthetic photon flux at 300 µmol/s and 500 µmol/m^2/s, respectively. The leaf chamber block temperature was set at 25 °C and the relative humidity at 40–60%. All measurements of fully unfolded leaves with green tissues were replicated three times.

The water use efficiency was calculated as a ratio between the net photosynthetic rate and the transpiration rate. The CO_2 assimilation rate (A) is a function of the intercellular CO_2 concentration (Ci) curve (A-Ci curve) and the A response to the light intensity curve. They were measured in 52 and 59 DAT Kimchi leaves, respectively, using a portable photosynthesis system (Li 6400XT, LI-COR Co., Inc., USA). The fully expanded leaves were clamped onto a 6-cm^2 leaf chamber and the light was provided by a sensor head (6400-02B LED, LI-COR Co., USA). The relative humidity in the leaf chamber ranged from 70 to 80% and the block temperature was maintained at 25 °C. For the An-Ci curve, gas exchange responses to the various CO_2 concentrations ranged from 50 to 1,500 µmol/mol. They were measured at 500 µmol/m^2/s photosynthetic photon flux (PPF) with a 10% ratio of blue light to maximize the stomatal aperture. The light response curves were measured at irradiance levels of 1800, 1500, 1200, 1000, 800, 500, 250, 100, 50, and 0 µmol/ m^2/s PPF with 400 µmol/mol CO_2 concentration. Three replicates per treatment were performed. The calculation of CO_2, light saturation, and compensation points were done with a regression analysis using a descriptive model (exponential rise to maximum, three parameters).

Results

Profiles of air temperature in a semi-closed plastic tunnel

The outside GTG environment factors: radiation intensity, air temperature, relative humidity, wind speed and direction, and precipitation in the cloudy and sunny days are represented in Fig. 5. The total integral solar radiation was 0.5 and 9.4 MJ/m^2/d for the cloudy and sunny days, respectively. The maximum radiation intensity was approximately 25 and 452 W/m^2, respectively. The daily mean temperature of the cloudy day outside GTG was 7.1 °C, while for the sunny day it was 6.1 °C. The relative humidity in the cloudy day was 90.4%, the average wind speed was 2.5 m/s with southwest direction, and the precipitation was 11.2 mm/d. However, the relative humidity outside GTG in the sunny day was 69.1%, the wind speed was 1.1 m/s, and the wind direction was mainly southeast.

The daily mean temperature in the cloudy day was 7.5 °C–8.8 °C in zone A of the GTG (Table 3). The temperature difference between zone A and B was approximately 3.0 °C. The maximum temperature difference of GTG was 5.7 °C, which means a well-controlled set point (6 °C difference between GTG outside and most-inside GTG conditions). The particular reason that the average daily temperature measured at the farthest distance from the outside was lower (about 0.7 °C) compared to the previous position is the installation of a fan that leads to temperature difference and heat loss. Also, the temperature

difference between day and night occurred according to the house distance similar to the daily average temperature result. On the sunny day, the daily mean temperature close to the outside of the GTG was 6.3 °C–8.0 °C, 8.3 °C–9.2 °C, and 9.8 °C–10.9 °C in A, B, and C zones, respectively. In the C zone, which was 15.6 m inside GTG, or away from the outside environment, the daily mean temperature was up to 4.3 °C higher than that of A zone. Besides, the temperature difference between zone A and zone B was about 2.9 °C and the temperature difference between zone B and zone C was 1.7 °C. The temperature gradient in the sunny day was not well pronounced inside the GTG. The temperature difference between the photo and dark periods was similar to the daily mean temperature trend. However, the temperature gradient manifestation in the GTG was reduced in the sunny day. Even after a month of continuously collecting and analyzing data, it was obvious that the GTG temperature gradient is manifested according to the distance from the outside environment (data not shown).

Figures 6 and 7 represent the daily change of vertical temperature distribution measured in the same points outside and inside GTG. At a distance of 0.4 m from the ground, the temperature gradient changes according to the distance from the GTG outside, which when centered at noon during the day was up to 6 °C. The temperature difference in the house center was most stable. However, on both sides of the house (0.75 m from the outside), the temperature gradient was not completely pronounced. There were some temperature change waves due to external heat loss. The tendency was worse at 0.8 and 1.2 m above the ground. The most stable temperature gradient is shown at 25 m from the outside of GTG and 0.4 m from the ground. It showed minimal differences—from 6.3 to 4.7 °C (Fig. 6-d, e, and f). In addition, the temperature at 0.8 m was 4.8 °C–5.9 °C and that at 1.2 m above ground was 5.1 °C–6.2 °C. However, on the sunny day (Fig. 5), at the two hours around noon, the GTG temperature gradient was unbalanced.

Validation Of Measured Data And Cfd Simulation Values

The CFD model was validated by comparing field monitoring data with CFD-computed results. The error of the CFD model was on average 1.120 °C with a standard deviation of 0.640 (Fig. 7). The air temperature of CFD simulation at 0.4 m height was relatively higher than the field temperature. Comparing the field experiment to the CFD model in terms of temperature and ventilation flow, it seems that the air entering through the pipe inlet of the CFD model was well supplied. CFD modeling was performed to provide hot air heated at the one side through pipe inlet based on the design capacity. The generated heat was relatively lower than the desired capacity, which was caused by the pressure generated in the field experiment. In the CFD model, the airflow was concentrated at the floor bottom. The hot air was also stagnated at the bottom, resulting in an overestimation of the air temperature at the 0.4 m height. The CFD model results, compared to the field monitoring data at the 0.8 m height, showed an average error of 0.597 °C with a standard deviation of 0.472. The average error at 1.2 m height was 0.459 °C with a standard deviation of 0.526 as shown in Figs. 8 and 9. The longitudinal air temperature gradient showed a similar pattern. The results of CFD and the field experiment show that the CFD model can reproduce a reasonable airflow pattern compared with the field experiment. The average temperature for each length compared between the field and CFD data was 0.1025 of RMSE and 0.7403 of MAE.

Figure 10 shows the comparison of air temperatures between field measurements and CFD-computed results used for CFD validation at the same sampling locations. There is a relative similarity between field and CFD-computed results with R^2 = 0.784. According to the height analysis, the slopes showed 1.097 at the 0.4 m height and 0.970 at the 1.2 m height. This is a reasonable difference considering the unpredictable field conditions in comparison to the CFD simulation, which is ideal with its steady-state condition. At the 1.2 m height, the CFD-computed air temperature was relatively lower compared to the field-monitoring results. This is due to the warm air in the field greenhouse that was stagnated during the whole experimental period. At the 0.4 m height, the CFD results showed relatively higher air temperature compared to the field monitoring data. This is probably caused by the airflow pattern that was concentrated near the floor surface and the pipe inlets blowing hot air. Nevertheless, the difference between field and CFD results were negligible. The CFD model was able to simulate the field conditions with very high accordance.

Cfd Simulation In Regional Thermal Condition

Figure 12 shows the thermal distribution of the experimental greenhouse temperature gradient measured at a selected period for CFD model validation. Figure 13 shows the thermal distribution computed by the CFD model at the same initial conditions, which represents almost the same air temperature distributional pattern. Temperature gradients in field experiments showed 4.60 °C, 4.52 °C, and 5.62 °C at 0.4, 0.8, 1.2 m heights, respectively. The measurements were based on the temperature difference between six points near the inlet opening and six points near exhaust fans. The CFD-computed results also showed almost similar results. They confirmed that the air temperature can be maintained between 13 °C–15 °C through the half greenhouse. The airflow pattern computed by CFD showed relatively parallel results to the greenhouse. This was achieved by creating a negative pressure formed by the exhausting fans, which were installed on the other sidewall (Fig. 14). Since the incoming wind in the field experiment has entered in irregularly through the open wall, the CFD-computed airflow pattern and the thermal gradient were more uniform.

GTG application for the growth and photosynthesis characteristics of Kimchi cabbage

The growth of Kimchi cabbage was evaluated according to three different GTG temperature zones (A, B, and C). The daily mean temperatures in zone A, B, and C during the Kimchi cabbage cultivation period (60 days after transplanting) were 20.3 °C, 22.7 °C, and 25.1 °C, respectively (data not shown). The maximum leaf length, leaf number, leaf area, fresh weight, stomatal conductivity, and leaf temperature were significantly different. However, there was no significant difference in leaf width and SPAD value (Table 6). Zone A growth conditions are closest to the outside. It had the lowest growth rate (leaf growth, leaf area, and fresh weight) among treatments and the stomatal conductivity decreased by 98.9% compared to other higher-temperature zones in GTG. In particular, the stomatal conductivity of Kimchi cabbage leaves increased significantly along the temperature gradient. There was a significant difference in the net photosynthetic rate, transpiration rate, and Ci concentration along the temperature gradient, too (Table 7). The net photosynthetic rate increased in zones B and C where the temperature was high, while WUE of the Kimchi cabbage grown at low temperature (zone A) was 4.3 times higher than in the zone C.

Table 6
Camparsion of Kimchi cabbage growth and stomatal conductance along the temperature gradient (n = 3)

Cultivation position	Leaf width (cm/plant)	Leaf length (cm/plant)	Number of leaves	Leaf area (cm^2/plant)		Fresh weight (g/plant)		SPAD value	Stomal conductance ($mmol/m^2/s$)	Leaf temp. (°C)
A (Ambient)	24.6a[z]	50.8b	56b	19,973	b	1949.8	b	34.1a	144.5b	13.4c
B (A + 3 °C)	33.1a	56.5a	71a	29,127	a	3159.3	a	32.9a	184.1b	15.9b
C (A + 6 °C)	29.8a	56.3a	70a	24,598	ab	2536.0	ab	34.2a	290.6a	18.7a
Significance[y]	ns	**	**	*		*		ns	**	***

[z]The letters represent the significance by LSD test at p = 0.05.

[y]ns = not significant; *P ≤ 0.05, **P ≤ 0.01, ***P ≤ 0.001.

Table 7
Evaluation of Kimchi cabbage leaf photosynthesis along the temperature gradient (n = 3) at DAT

Cultivation position	Net Pn ($\mu mol \cdot m^{-2} \cdot s^{-1}$)	Tr ($mmol \cdot m^{-2} \cdot s^{-1}$)	WUR	gs ($mmol \cdot m^{-2} \cdot s^{-1}$)	Ci ($\mu mol \cdot mol^{-1}$)
A (Ambient)	13.6b[z]	3.2b	4.3a	235.4b	262.4b
B (A + 3 °C)	18.5a	6.7a	3.0b	742.8a	297.0a
C (A + 6 °C)	18.6a	7.4a	2.6b	750.6a	300.5a
Significance[y]	*	*	*	*	*
[z]The letters represent the significance by LSD test at p = 0.05.					
[y]*P ≤ 0.05.					

There was a difference in the maximum saturation of Ci concentration, the maximum photosynthetic rate according to Ci concentration, and the exponential decay model $y = a + b \times \{1 - exp^{(-c \times x)}\}$. The regression analysis showed that the Kimchi cabbage in zone B was the highest, followed by the Kimchi cabbage grown in zone A. The area with the lowest maximum photosynthetic rate was zone C (Fig. 8-a). Among the regression equations of the A-Ci curve of zone A, Kimchi cabbage coefficients a, b, and c were − 4.7, 30.9, and 0.005, respectively. The coefficient of determination (r^2) was 0.9959. The regression coefficients a, b, and c of the A-Ci curve of zone B were − 5.4, 35.4, and 0.004, respectively (r^2 = 0.9755). In the zone C, the coefficients a, b, and c were − 5.9, 33.9, and 0.004, respectively (r^2 = 0.9985). The CO_2 compensation point/saturation point of Kimchi cabbage leaves in zones A, B, and C were 33/369, 41/405, and 48/461 µmol/mol, respectively. As the light intensity increased, the photosynthetic rate increased in all treatments (Fig. 8b). The light curve of zone C, which had the optimal temperature for Kimchi cabbage, was most pronounced. The maximum photosynthetic rate decreased when the temperature decreased below the optimal growth temperature of Kimchi cabbage. The Kimchi cabbage light compensation/saturation point in zones A, B, and C were − 21/647, 8/468, and − 18/1008 µmol/ m^2/s, respectively.

Discussion

Intergovernmental Panel on Climate Change (IPCC) published climate change (CC) models that simulate air temperature suggesting that it will rise with 1 °C to 4 °C by the end of the 21st century due to increased greenhouse gas emissions in the atmosphere. When designing and implementing a GTG, the representative concentration pathway (RCP) 8.5 CC scenario of the Korean Meteorological Administration should be taken into account. This report confirmed that after 100 years, the temperature will increase by approximately 6 °C from the current average level without any mitigation policy applied. As a result of the temperature deviation profiling of GTG, the temperature difference set in the control program was predicted very accurately (Figs. 4 and 5, Table 3). There are many approaches regarding the temperature gradient and CO_2 concentration change in semi-open type greenhouses. The research of climate change impact on crop production using GTG showed that the temperature gradients in a partially shaded large greenhouses were created with evaporative cooling pads [17]. Those facilities had well-controlled set points. There were similar works on gradients of temperature, humidity, and CO_2 for fan-ventilated greenhouses [18]. These studies focused on the night-time thermal gradients in the greenhouse using computational thermal dynamics [19]. Other similar studies have been conducted on sunlit plant growth chambers with controlled-environment [11]. There are also studies regarding the construction of large-scale semi-field facilities to study genotypic differences in deep-root growth and resource acquisition [20]. Those studies claimed that accuracy and precision are important for the device or facility's performance. Therefore, this has become a major task for the assessment of crop impacts and vulnerability due to climate change.

In studying the response of agriculture research fields to climate change, it is necessary to rely on growth models for the study of crop physiological and biochemical reactions. Also, the prediction of crop production should be done in terms of statistical and mathematical models, which to be calibrated and verified. In such cases, a chamber using artificial light is mainly used, or agricultural statistics for national surveys are occasionally used. However, calibration and verification methods can lead to errors in the calculation of actual crop biomass. GTG was used in various crops as utilization equipment for correcting and verifying such errors. Using of GTG experimental facilities under high temperature and drought conditions led to significantly and consistently increased pH due to decreases in malic acid of grapevine [21]. When plants were grown under elevated CO_2, the largest increase was observed in leaf (white) and root (red) growth. An increase in the mean temperature with 4 °C had no consequences on the vegetative growth of grapevine. Yield and yield-related traits were unaffected by the climate change scenario [3]. Previous research revealed that an increase in air temperature, CO_2 concentration, and precipitation significantly disturbed plant growth and reduced the yield of horticultural crops [1, 5, 7–9, 22–25]. Especially, using the extreme weather simulators [26] have documented the impact of moderate and extreme climate change scenarios on growth, morphological features, photosynthesis, and fruit production of hot pepper. Similar work has dealt with the temperature gradient and air–soil as a factor in the optimization of net photosynthesis in whole plants [27]. Finally, stem juice production of the C4 sugarcane (*Saccharum officinarum*) is enhanced by growth at double-ambient CO2 and high temperature [28].

Compared to zone B, the fresh weight was lower in zone C, which had the highest temperature in the GTG. This was due to the approximately higher temperature (with about 3 °C) compared to the Kimchi cabbage optimal cultivation temperature (average 20 °C), leading to partly physiological damage to the head formation (Table 6). The combination of elevated temperature and CO_2 concentration stimulated leaf dry weight reduction of Kimchi cabbage. It decreased about 3-fold compared to that only exposed to elevated CO_2. A drastic decrease was also observed in stomatal conductance, internal CO_2, and photosynthesis rate [22]. A temperature increase from 28 °C to 32 °C resulted in less leaf calcium, magnesium, and manganese concentrations (dry weight basis) in pakchoi without significant changes in shoot dry weight, suggesting potential negative effects of the elevated temperature on pakchoi leaf nutrient status [23]. The moderate and extreme climate change (CC) treatments led to physiological disorders in terms of tip burn leaves, while the control plants with normal climate condition applied by weather of primary production area had the greatest yield among the studied plants. The yield of moderated treatment 65% reduction observed in moderate CC treatment plants. The CC scenarios retarded the growth of Kimchi cabbage and negatively affected leaf morphology, photosynthesis efficiency, and yield [29]. In general, Kimchi cabbages are harvested around 50 to 100 days after sowing, depending on the cultivar, cropping type, cultivation season, and the prevailing weather conditions. Kimchi cabbage is represented as a cool-season crop, thus that will not occur head formation when the daily mean air temperature is over 25 °C. The net photosynthetic rate increased in high-temperature zones, while WUE of Kimchi cabbage grown at low temperature (zone A) was 4.3 times higher than in the zone where the temperature was highest (Table 7). The efficiency of photosynthetic system improved under warm temperature. However, WUE in cool season crops is normally strengthen by optimal temperatures [27, 29, 30]. Regarding the A-Ci and light curves (Fig. 8), the maximum net photosynthetic rate of Kimchi cabbage in zone B was highest. It was followed by the Kimchi cabbage grown in zone A. The area with the lowest maximum photosynthetic rate was zone C. Previous research revealed that the maximum carboxylation rate, maximum rate of electron transport, and triose phosphate utilization rate of the higher temperature treatment plants were significantly lower than those of the control [7, 8, 22, 26, 29, 31, 32]. It was confirmed that the GTG can be applied to climate change response and adaptation studies. Therefore, it is expected that this study can also be used to evaluate the vulnerability and impact of climate change in open-ended vegetables, especially by utilizing GTG.

Conclusions

The GTG was well-designed to create a temperature gradient. The cultivation experiment of Kimchi cabbage, a low-temperature crop, was useful to study the growth and physiological response to the temperature gradient. CFD can simulate

the temperature gradient in tunnel-type greenhouses and predict the temperature difference for equipment with different specifications. It is expected that these facilities will be used to conduct climate change-related studies for assessments of crop production area optimization, crop physiological responses to temperature, and vulnerability assessment of crop production under increasing temperatures or extreme weather. The CFD simulation model can be used effectively to understand airflow patterns and thermal distribution in the greenhouse temperature gradient. CFD simulation showed similar results to the field experiment since the temperature difference was only five degrees. CFD model was validated by computation of about 90 air temperature data that were compared with the field measurements. This resulted in good agreement between the analysis of airflow patterns and thermal distribution. After changing the boundary conditions near the entrance, it is possible to simulate the internal environment according to a preliminary intention. Then, the advanced ventilation system, including heating and ventilation structures, can be applied to an experimental greenhouse for maintaining internal environmental conditions. Using the greenhouse temperature gradient with the CFD modeling technique allows us to better comprehend the growth rate of plants such as cabbage.

Abbreviations

CC: Climate Change; GTG: Greenhouse Temperature Gradient; CFD: Computational Fluid Dynamics; Pn: Net Photosynthetic Rate; Ci: intercellular carbon dioxide concentration; gs: stomatal conductance, Tr: transpiration rate; WUR: water use efficiency rate; DAT: Days After Transplanting; RCP: Representative Concentration Pathway.

Declarations

Ethics approval and consent to participate

Not applicable.

Consent for publication

Not applicable.

Availability of data and materials

The raw data from all experiments, as well as the material used in this manuscript, can be obtained from the corresponding author upon reasonable request.

Competing interests

The authors declare that they have no competing interests.

Funding

This work was carried out with the support of the “Cooperative Research Program for Agriculture, Science & Technology (Project No. PJ01196501)”, Rural Development Administration, Republic of Korea. The funder took part in the design of the study; collection, analysis and interpretation of the data; and writing of the manuscript.

Authors’ contributions

SHW and SWL performed the experiment. SKK and HJL analyzed the data and wrote the manuscript. IHS designed the experiment, analyzed the data, and revised the manuscript. All authors have read and approved the manuscript before submit

Acknowledgments

We are grateful to Suran An for drawing the GTG 3D structures and to Jonghyun Kim for providing the control algorisms in GTG environmental system.

References

1. Hakala K, Mela T, Laurila H, Kaukoranta T. Arrangement of experiments for simulating the effects of elevated temperatures and elevated CO2 levels on field-sown crops in Finland. Agricultural Food Science in Finland. 1996;5:25–47. doi:10.23986/afsci.72728.
2. Kawasaki Y, Yoneda Y. Local temperature control in greenhouse vegetable production. Horticulture Journal. 2019;88:305–14. doi:10.2503/hortj.UTD-R004.
3. Kizildeniz T, Irigoyen JJ, Pascual I, Morales F. Simulating the impact of climate change (elevated CO_2 and temperature, and water deficit) on the growth of red and white Tempranillo grapevine in three consecutive growing seasons (2013–2015). Agric Water Manag. 2018;202:220–30. doi:10.1016/j.agwat.2018.02.006.
4. Kizildeniz T, Mekni I, Santesteban H, Pascual I, Morales F, Irigoyen JJ. Effects of climate change including elevated CO2 concentration, temperature and water deficit on growth, water status, and yield quality of grapevine (*Vitis vinifera* L.) cultivars. Agric Water Manag. 2015;159:155–64. doi:10.1016/j.agwat.2015.06.015.
5. Allen LH, Vu JCV. Carbon dioxide and high temperature effects on growth of young orange trees in a humid, subtropical environment. Agric For Meteorol. 2009;149:820–30. doi:10.1016/j.agrformet.2008.11.002.
6. Salazar-Parra C, Aranjuelo I, Pascual I, Erice G, Sanz-Saez A, Aguirreolea J, Sanchez-Diaz M, Irigoyen JJ, Araus JL, Morales F. Carbon balance, partitioning and photosynthetic acclimation in fruit-bearing grapevine (*Vitis vinifera* L. cv. Tempranillo) grown under simulated climate change (elevated CO_2, elevated temperature and moderate drought) scenarios in temperature gradient greenhouses. J Plant Physiol. 2015;174:97–109. doi:10.1016/j.jplph.2014.10.009.
7. Oh S, Moon KH, Son IC, Song EY, Moon YE, Koh SC. Growth, photosynthesis and chlorophyll fluorescence of Chinese cabbage in response to high temperature. Korean Journal of Horticultural Science Technology. 2014;32:318–29. doi:10.7235/hort.2014.13174.
8. Oh S, Moon KH, Song EY, Son IC, Koh SC. Photosynthesis of Chinese cabbage and radish in response to rising leaf temperature during spring. Horticulture Environment Biotechnology. 2015;56:159–66. doi:10.1007/s13580-015-0122-1.
9. Qian T, Dieleman JA, Elings A, De Gelder A, Marcelis LFM. Response of tomato crop growth and development to a vertical temperature gradient in a semi-closed greenhouse. Journal of Horticultural Science Biotechnology. 2015;90:578–84. doi:10.1080/14620316.2015.11668717.
10. Morales F, Pascual I, Sanchez-Diaz M, Aguirreolea J, Irigoyen JJ, Goicoechea N, Antolin MC, Oyarzun M, Urdiain A. Methodological advances: Using greenhouses to simulate climate change scenarios. Plant Sci. 2014;226:30–40. doi:10.1016/j.plantsci.2014.03.018.
11. Liu L, Hoogenboom G, Ingram KT. Controlled-environment sunlit plant growth chambers. Crit Rev Plant Sci. 2000;19:347–75. doi:10.1016/s0735-2689(00)80008-8.
12. Bello-Robles JC, Begovich O, Ruiz-Leon J, Fuentes-Aguilar RQ. Modeling of temperature distribution of a greenhouse using finite element differential neural networks. Kybernetika 2018, 54, 1033–1048, doi:10.14736/kyb-2018-5-1033.
13. Lee I-B, Bitog JPP, Hong S-W, Seo I-H, Kwon K-S, Bartzanas T, et al. Thepast, present and future of CFD for agro-environmental applications. Comput Electron Agric. 2013;93:168–83. http://dx.doi.org/10.1016/j.compag.2012.09.006.
14. 10.1016/j.enbuild.2016.05.014
Benni S, Tassinari P, Bonora F, Barbaresi A, Torreggiani D. (2016) Efficacy of greenhouse natural ventilation: Environmental monitoring and CFD simulations of a study case. *Energy and Bu8ildings, 125, 276–286.* http://dx.doi.org/10.1016/j.enbuild.2016.05.014.
15. Kim R-W, Hong S-W, Lee I-B, Kwon K-S. (2017). Evaluation of wind pressure acting on multi-0span greenhouses using CFD technique, Part 2: Application of the CFD model. Biosys Eng, 164.

https://doi.org/10.1016/j.biosystemseng.2017.09.011.

16. Villagrán EA, Romero EJB, Bojacá CR. Transient CFD analysis of the natural ventilation of three types of greenhouses used for agricultural production in a tropical mountain climate. Biosys Eng. 2019;188:288–304. https://doi.org/10.1016/j.biosystemseng.2019.10.026.
17. Kittas C, Bartzanas T, Jaffrin A. Temperature gradients in a partially shaded large greenhouse equipped with evaporative cooling pads. Biosys Eng. 2003;85:87–94. doi:10.1016/S1537-5110(03)00018-7.
18. Teitel M, Atias M, Barak M. Gradients of temperature, humidity and CO_2 along a fan-ventilated greenhouse. Biosys Eng. 2010;106:166–74. doi:10.1016/j.biosystemseng.2010.03.007.
19. Espinal-Montes V, Lopez-Cruz IL, Rojano-Aguilar A, Romantchik-Kriuchova E, Ramirez-Arias A. Determination of night-time thermal gradients in a greenhouse using computational thermal dynamics. Agrociencia. 2015;49:233–47.
20. Svane SF, Jensen CS, Thorup-Kristensen K. Construction of a large-scale semi-field facility to study genotypic differences in deep root growth and resources acquisition. Plant Methods 2019, 15, doi:10.1186/s13007-019-0409-9.
21. Kizildeniz T, Pascual I, Irigoyen JJ, Morales F. Using fruit-bearing cuttings of grapevine and temperature gradient greenhouses to evaluate effects of climate change (elevated CO_2 and temperature, and water deficit) on the cv. red and white Tempranillo. Yield and must quality in three consecutive growing seasons (2013–2015). Agric Water Manag. 2018;202:299–310. doi:10.1016/j.agwat.2017.12.001.
22. Choi EY, Seo TC, Lee SG, Cho IH, Stangoulis J. Growth and physiological responses of Chinese cabbage and radish to long-term exposure to elevated carbon dioxide and temperature. Horticulture Environment Biotechnology. 2011;52:376–86. doi:10.1007/s13580-011-0012-0.
23. Hwang SG, Chao HC, Lin HL. Differential responses of pak choi and edible amaranth to an elevated temperature. HortScience. 2018;53:195–9. doi:10.21273/hortsci12667-17.
24. Lee HJ, Lee SG, Kim SK, An S, Lee JH, Lee HS, Kim CW, Kwon YS, Han JW. Effects of high-temperature and soil moisture conditions on the physiological response of onion. Horticultural Science Technology. 2019;37:571–8.
25. Lee HJ, Lee SG, Kim SK, Mum BH, Lee JH, Lee HS, Kwon YS, Han JW, Kim CW. Effects of combination of air temperature and soil moisture contents on growth, clove initiation, physiological disorders, and yield of garlic. Protected Horticulture Plant Factory. 2018;27:191–8.
26. Lee SG, Kim SK, Lee HJ, Lee HS, Lee JH. Impact of moderate and extreme climate change scenarios on growth, morphological features, photosynthesis, and fruit production of hot pepper. Ecology Evolution. 2018;8:197–206. doi:10.1002/ece3.3647.
27. Kurets VK, Drosdov SN, Popov EG, Talanov AV, Dembo ED. The temperature gradient air-soil as a factor in the optimization of net photosynthesis in whole plants. Russ J Plant Physiol. 2003;50:72–8. doi:10.1023/a:1021940618961.
28. Vu JCV, Allen LH. Stem juice production of the C-4 sugarcane (*Saccharum officinarum*) is enhanced by growth at double-ambient CO_2 and high temperature. J Plant Physiol. 2009;166:1141–51. doi:10.1016/j.jplph.2009.01.003.
29. Lee SG, Kim SK, Lee HJ, Choi CS, Park ST. Impacts of climate change on the growth, morphological and physiological response, and yield of Kimchi cabbage leaves. Horticultural Environmental Biotechnology. 2016;57:470–7.
30. Diaz-Perez JC, John KS. Bell Pepper (*Capsicum annum* L.) under colored shade nets: plant growth and physiological responses. HortScience. 2019;54:1795–801. doi:10.21273/hortsci14233-19.
31. Yuan LY, Yuan YJ, Liu S, Wang J, Zhu SD, Chen GH, Hou JF, Wang CG. Influence of high temperature on photosynthesis, antioxidative capacity of chloroplast, and carbon assimilation among heat-tolerant and heat-susceptible genotypes of nonheading Chinese cabbage. HortScience. 2017;52:1464–70. doi:10.21273/hortsci12259-17.
32. 10.21273/hortsci.49.2.166
Kitta E, Katsoulas N, Kandila A, Gonzalez-Real MM, Bailie A Photosynthetic acclimation of sweet pepper plants to screenhouse conditions. HortScience 2014, 49, 166–172, doi:10.21273/hortsci.49.2.166.

Figures

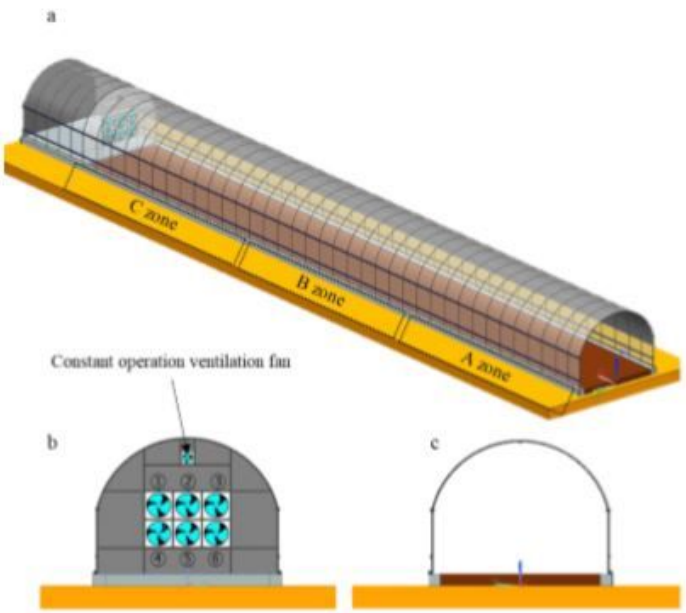

Figure 1

Structure of the temperature gradient house with the semi-closed plastic tunnel. a: scheme of all parts, b: the north side of ventilation air fans, and c: open space for the inflow of fresh outside air.

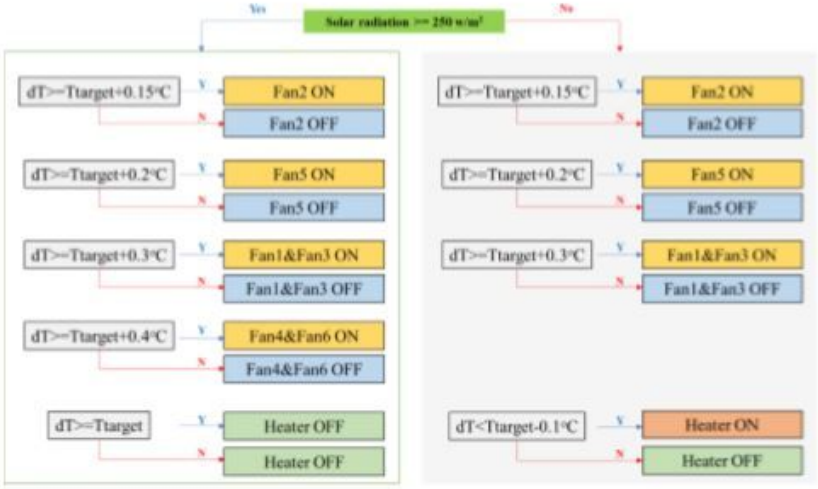

Figure 2

Controlling algorithm of the heater and ventilation fans intended to maintain the air temperature of the greenhouse temperature gradient.

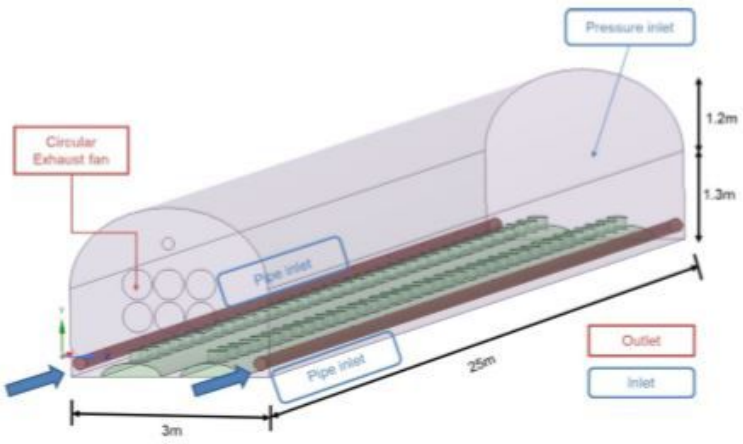

Figure 3

Schematic diagram of the experimental greenhouse with temperature difference for CFD simulation.

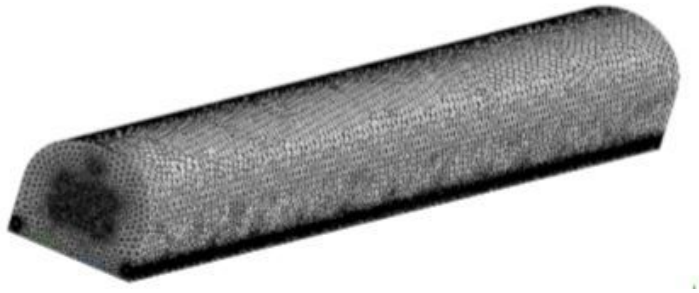

Figure 4

Mesh design of the experimental greenhouse using CFD. Denser meshes were used for the aerodynamically important area near the ventilation system and obstacles.

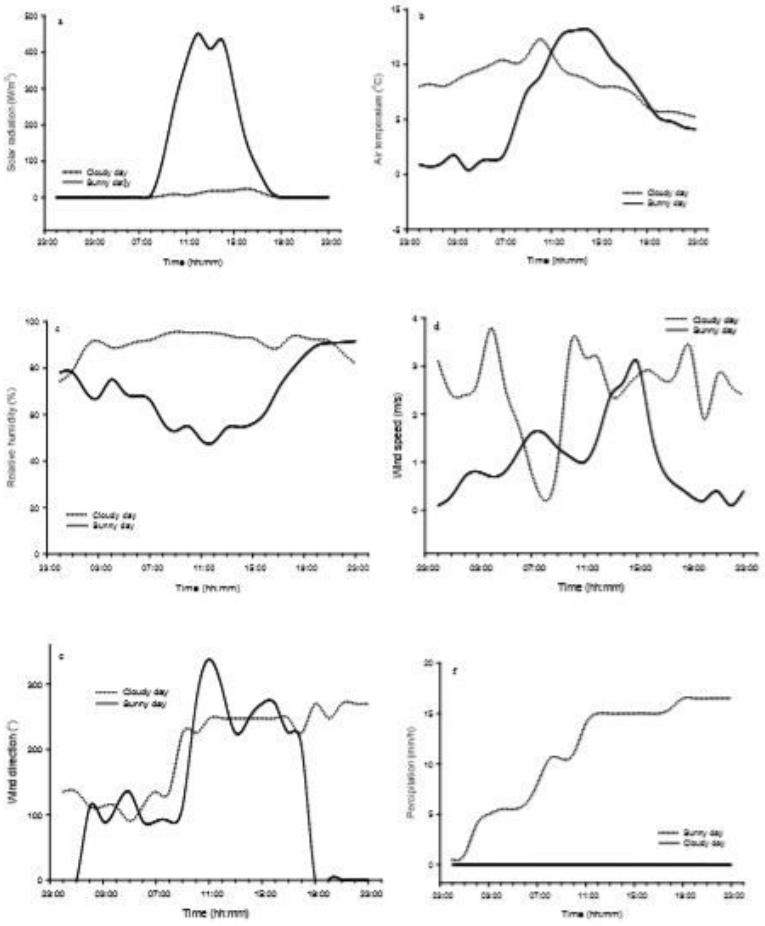

Figure 5

Outside environmental conditions during the measurement of air temperature for validation of CFD simulation data. a: solar radiation, b: air temperature, c: relative humidity, d: wind speed, e: wind direction, and f: precipitation.

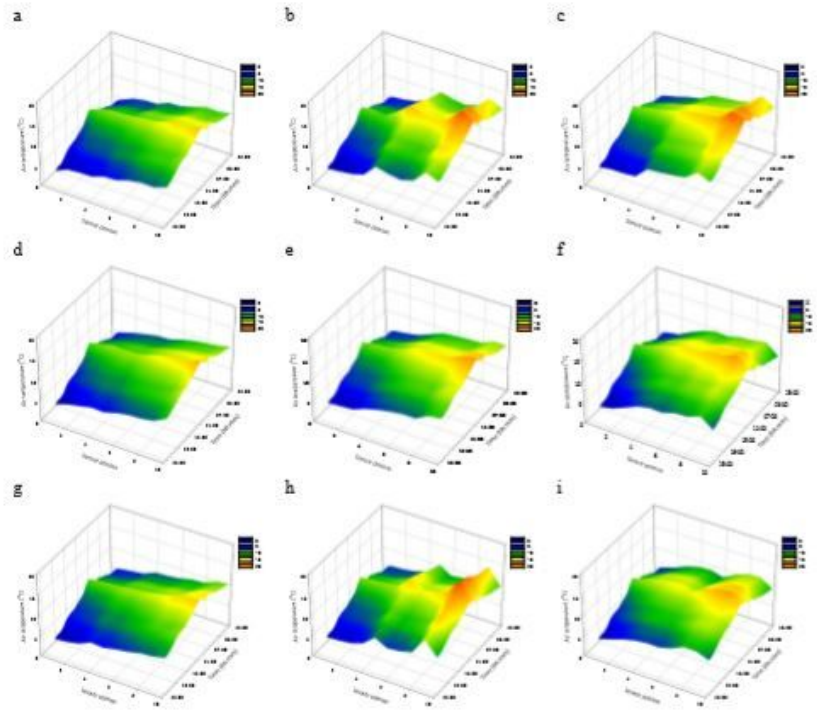

Figure 6

Profiles of daily air temperature on the cloudy day with 90 points. a, b, and c represent 0.75 m from west bound and each vertical point (bottom, middle, and top), respectively. d, e, and f represent 1.5 m from west bound. g, h, and i represent 2.25 m from west bound. d, e, f, g, h, and i each vertical point as followed by a, b, and c.

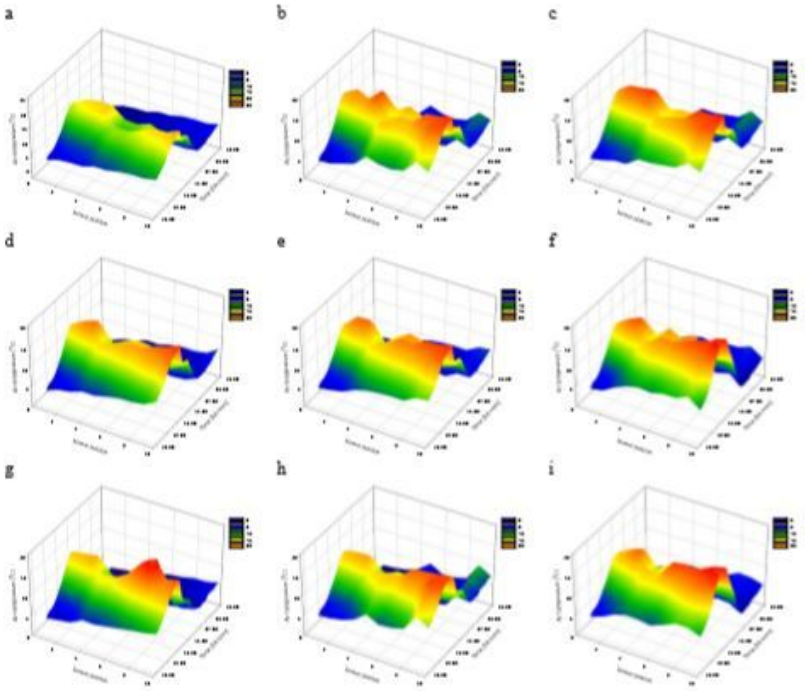

Figure 7

Profiles of daily air temperature on the sunny day with 90 points. a, b, and c represent 0.75 m from west bound and each vertical point (bottom, middle, and top), respectively. d, e, and f represent 1.5 m from west bound. g, h, and i represent 2.25 m from west bound. d, e, f, g, h, and i each vertical point as followed by a, b, and c.

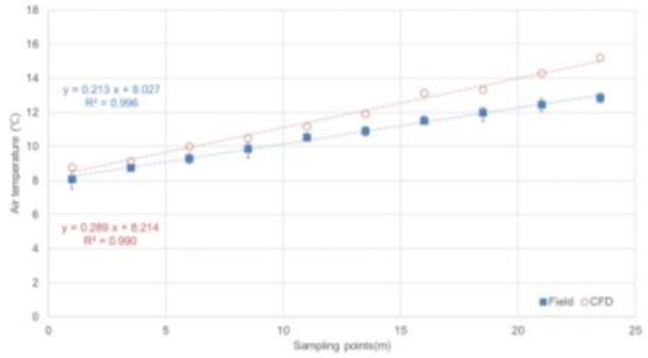

(a) 0.4 m above the floor

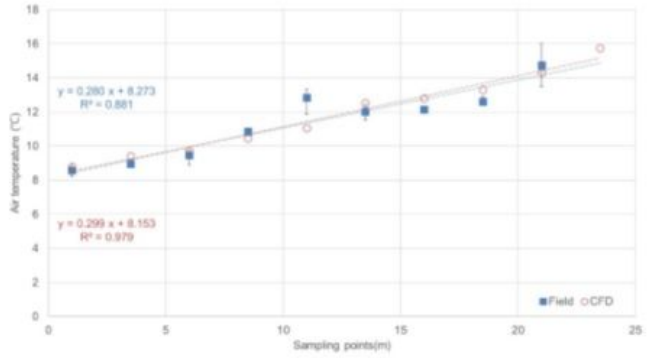

(b) 0.8 m above the floor

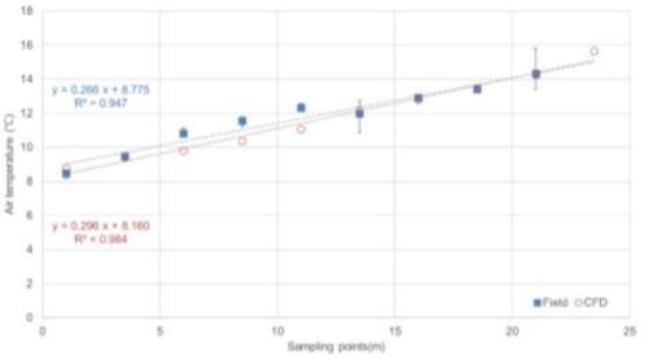

(c) 1.2 m above the floor

Figure 8

Comparison of air temperature distribution measured by field monitoring and computed by CFD simulation at: (a) 0.4 m, (b) 0.8 m, and (c) 1.2 m heights above the floor.

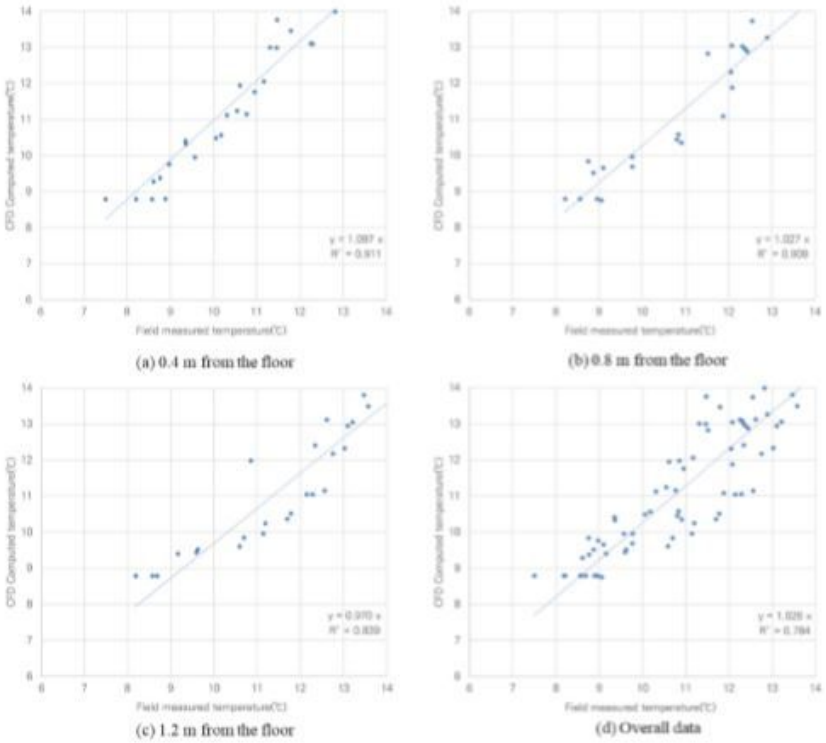

Figure 9

Validation of CFD simulation by field monitoring data according to the measurement points: (a) 0.4 m, (b) 0.8 m, and (c) 1.2 m height; (d) overall data.

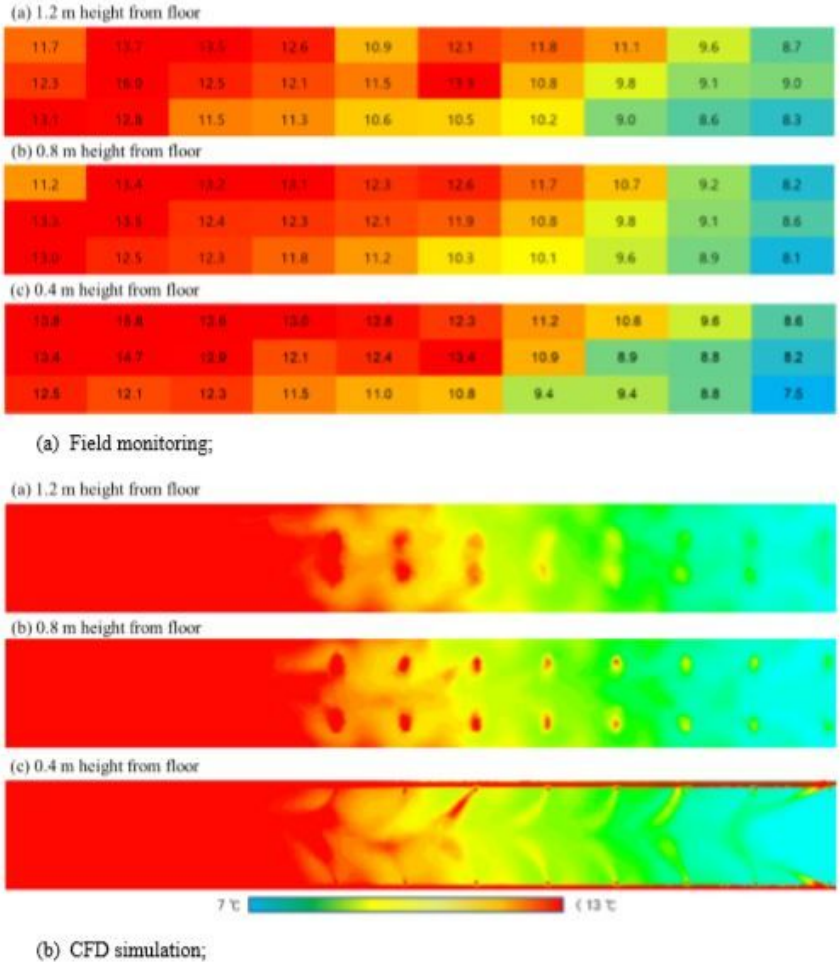

Figure 10

Air temperature distribution. (a) measured by field monitoring, and (b) computed by CFD.

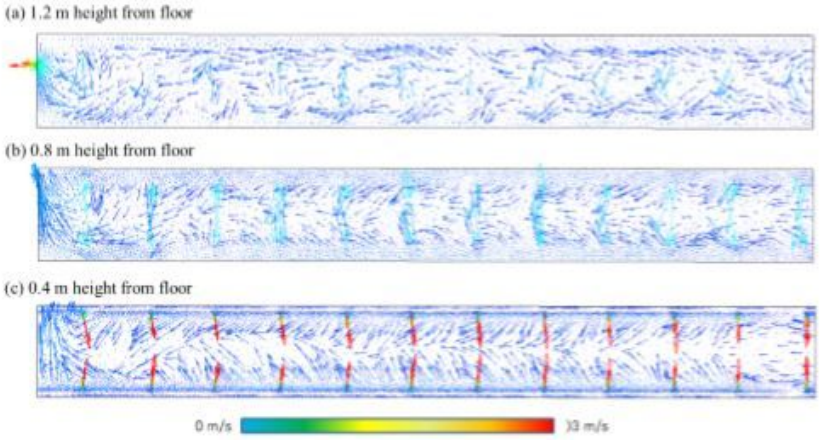

Figure 11

Airflow pattern computed by CFD simulation at the three different heights.

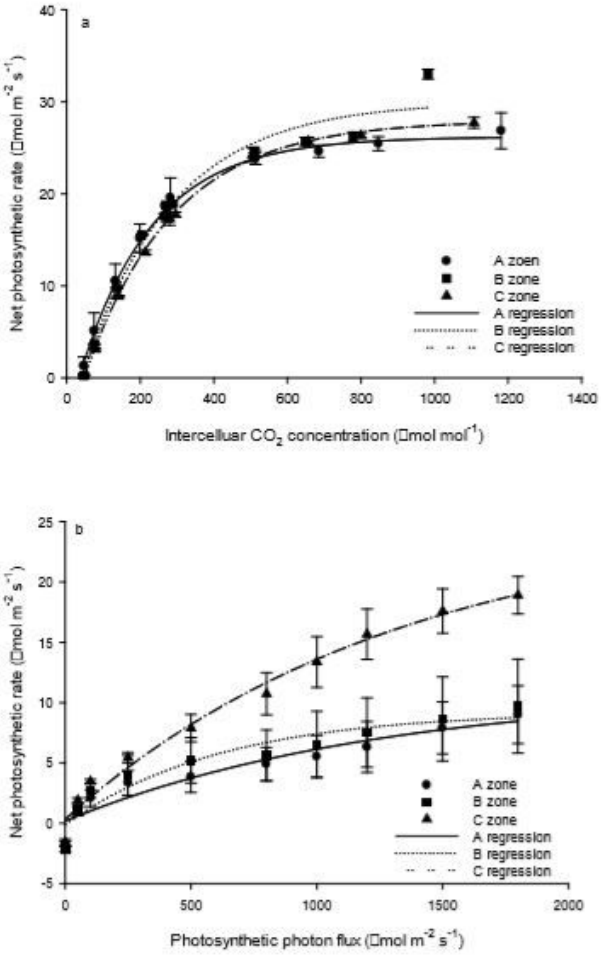

Figure 12

Intercellular CO2 concentration/assimilation and light reaction curves of Kimchi cabbage in different positions along the temperature gradient.